# Goldilocks calcium and the mitochondrial respiratory chain: too much, too little, just right

Eloisa A. Vilas-Boas*, João Victor Cabral-Costa, Vitor M. Ramos, Camille C.C. da Silva, Alicia J. Kowaltowski*.

Departamento de Bioquímica, Instituto de Química, Universidade de São Paulo, São Paulo, SP, Brazil.

*To whom correspondence should be addressed:
Tel.: +55 11 30912922
Email: elovilasboas@usp.br, alicia@iq.usp.br

**Running title:** Calcium and mitochondrial respiratory regulation.

**Keywords:** calcium transport, mitochondria, electron transfer chain, oxidative phosphorylation.

**Abstract**

Calcium ($Ca^{2+}$) is a key regulator in diverse intracellular signaling pathways, and has long been implicated in metabolic control and mitochondrial function. Mitochondria can actively take up large amounts of $Ca^{2+}$, thereby acting as important intracellular $Ca^{2+}$ buffers and affecting cytosolic $Ca^{2+}$ transients. Excessive mitochondrial matrix $Ca^{2+}$ is known to be deleterious due to opening of the mitochondrial permeability transition pore (mPTP) and consequent membrane potential dissipation, leading to mitochondrial swelling, rupture and cell death. But moderate $Ca^{2+}$ within the organelle can directly or indirectly activate mitochondrial matrix enzymes, possibly impacting on ATP production. However, *in vitro* studies involving the regulation of mitochondrial enzymes by $Ca^{2+}$ may not uncover its full effects on oxidative phosphorylation. Here, we aimed to determine if extra or intramitochondrial $Ca^{2+}$ modulate oxidative phosphorylation in mouse liver mitochondria and intact hepatocytes. We found that isolated mitochondria present increased respiratory control ratios (a measure of oxidative phosphorylation efficiency) when incubated with low and medium $Ca^{2+}$ concentrations in the presence of complex I-linked substrates pyruvate plus malate and α-ketoglutarate, respectively, but not complex II-linked succinate. In intact hepatocytes, both low and high cytosolic $Ca^{2+}$ led to decreased respiratory rates, while ideal rates were present under physiological conditions. High $Ca^{2+}$ decreased mitochondrial respiration in cells in a substrate-dependent manner, mediated by mPTP. Overall, our results uncover a Goldilocks effect of $Ca^{2+}$ on liver mitochondria, with specific "just right" concentrations that activate oxidative phosphorylation.

## 1. Introduction

Calcium ($Ca^{2+}$) is an important second messenger and participates in a myriad of cellular functions. Mitochondria are one of the central intracellular regulators of $Ca^{2+}$ homeostasis (1), as they can actively take up the ion down their electrochemical potential (2,3). While the affinity for $Ca^{2+}$ uptake is lower than for the endoplasmic reticulum (ER), mitochondria can absorb very large amounts of the ion from the cytosol (4-6). Mitochondria can also release $Ca^{2+}$, and are thus recognized as important rheostats for cytosolic $Ca^{2+}$ dynamics and signaling. Furthermore, mitochondria also participate in crosstalk signals between intracellular compartments, such as with the ER, through microdomains formed between both organelles in which ions have distinct concentrations and their exchange mediates inter-organelle communication (7).

$Ca^{2+}$ uptake across the inner mitochondrial membrane into the mitochondrial matrix occurs through the mitochondrial $Ca^{2+}$ uniporter complex (MCU) (8-10). The membrane potential generated by the electron transport chain (ETC), with a negative matrix charge, provides the electrochemical force necessary for positively charged ions, such as $Ca^{2+}$, to enter. $Ca^{2+}$ efflux from the mitochondrial matrix occurs through the $Na^{+}/Ca^{2+}$ exchanger (NCLX) (11), located in the inner mitochondrial membrane (IMM), and by a $Ca^{2+}/H^{+}$ exchanger, which may have been recently identified (12,13).

Mitochondrial $Ca^{2+}$ transients are believed to provide a link between cytosolic $Ca^{2+}$ signaling and the control of cellular energy demand by regulating ATP production. Pyruvate dehydrogenase, isocitrate dehydrogenase, and α-ketoglutarate dehydrogenase within the mitochondrial matrix have increased activities in the presence of $Ca^{2+}$, as uncovered through *in vitro* studies (14-17). For these activities to translate into enhanced oxidative phosphorylation *in vivo*, two conditions need to be met: first, the change in enzymatic activity promoted by $Ca^{2+}$ needs to be sufficient to overcome rate-limiting steps in oxidative phosphorylation and, second, $Ca^{2+}$ concentrations need to be below those that hamper mitochondrial function. Mitochondrial $Ca^{2+}$ overload leads to swelling of the organelle and opening of the mitochondrial permeability transition pore (mPTP), often culminating in loss of function and cell death (18-20). This process has been implicated in various diseases (21,22).

In theory, and when present at lower concentrations than those that lead to mPTP opening, $Ca^{2+}$ should activate mitochondrial electron transport and ATP production, but direct studies so far are limited to uncovering the modulation of isolated enzyme activity, and only show increases in substrate affinity, not maximal velocity. The effects of

changes in the affinity of these enzymes on overall mitochondrial metabolic pathway flux have not been determined. We explore this gap here, to determine if extra or intramitochondrial $Ca^{2+}$ modulates oxidative phosphorylation supported by different substrates in isolated mitochondria, focusing on the liver, since a rich metabolic regulation by $Ca^{2+}$ occurs in this tissue. We also explore how mitochondrial $Ca^{2+}$ transport influences oxidative phosphorylation in intact hepatocytes. Our results demonstrate that $Ca^{2+}$ concentrations greatly impact mitochondrial respiration, with a Goldilocks-type effect, in which both too much and too little $Ca^{2+}$ limit oxidative phosphorylation, but the "just right" concentration promotes significant activation.

## 2. Results

### *2.1. $Ca^{2+}$ increases liver oxidative phosphorylation efficiency in a substrate- and concentration-dependent manner*

To gain insight into the effects of extramitochondrial $Ca^{2+}$ addition on mitochondrial respiration, we used isolated mouse liver mitochondria in the presence of different substrates and measured oxygen consumption over time using an Oroboros high-resolution oxygraph. $Ca^{2+}$ was added at different concentrations, followed by additions of ADP (to induce oxidative phosphorylation, state 3), oligomycin (to inhibit ATP synthase and measure respiration dependent on the proton leak, state 4) and CCCP (to induce maximum electron transport). We determined residual $Ca^{2+}$ concentrations present after mitochondrial isolation daily, and then calculated the amount of $Ca^{2+}$ added so it was equal between biological replicates, classifying conditions as no added $Ca^{2+}$, low (2.4 ± 0.6 µM), medium (22.0 ± 2.4 µM) and high (52.9 ± 2.5 µM) added $Ca^{2+}$ concentrations.

Complex I substrates such as pyruvate and malate were chosen initially to study the effects of $Ca^{2+}$ on electron transport and oxidative phosphorylation, due to the known enhancement of pyruvate dehydrogenase (PDH) affinity in response to $Ca^{2+}$ signaling (14-17). $Ca^{2+}$ uptake traces with low and medium $Ca^{2+}$ concentrations are shown in Fig. 1A. The downward deflection in the curve within 2-3 min indicates a decrease in extramitochondrial $Ca^{2+}$ measured with the fluorophore $Ca^{2+}$ Green due to uptake by mitochondria (Fig. 1A). High $Ca^{2+}$ led to mitochondrial dysfunction with these substrates (Fig. S1A) and was thus not included in further experiments; $O_2$ consumption traces were measured using only low and medium $Ca^{2+}$ additions, and are shown as oxygen consumption rates (OCR) in Figs. 1B-D, and quantified results in panels E-H.

We found that the presence of low $Ca^{2+}$ concentrations strongly increased state 3 respiration, when oxidative phosphorylation is active (Fig. 1E). State 4 respiration, which occurs in the absence of ATP synthase and is limited by the inner membrane impermeability to protons, was stimulated by both low and medium $Ca^{2+}$ concentrations when supported by pyruvate and malate (Fig. 1F). The respiratory control ratio (RCR, Fig. 1G) is the ratio between state 3 and state 4 oxygen consumption, and is used as a proxy for oxidative phosphorylation efficiency, as it shows the relative stimulation of oxygen consumption by the production of mitochondrial ATP (23). We found that the RCR was increased at low but not medium $Ca^{2+}$ concentrations (Fig. 1G). This shows that oxidative phosphorylation supported by pyruvate and malate has a tight relationship with

mitochondrial $Ca^{2+}$, and is more effective within a very specific range of added extramitochondrial $Ca^{2+}$.

We investigated next if the increase in oxidative phosphorylation efficiency observed was dependent on mitochondrial $Ca^{2+}$ uptake or cycling, using pharmacological inhibitors of the MCU (Ruthenium red, RuRed), which prevents $Ca^{2+}$ uptake, and of the NCLX (CGP-37157, CGP), which prevents $Ca^{2+}$ extrusion from mitochondria (Fig. 1H). Both RuRed and CGP reversed the increase in RCR promoted by low $Ca^{2+}$ concentrations; this indicates that $Ca^{2+}$ must enter the mitochondrial matrix to exert this effect, as RuRed prevents this uptake. The effect of CGP could also indicate that increased RCRs are dependent on $Ca^{2+}$ cycling, as it inhibits $Ca^{2+}$ extrusion from mitochondria through $Ca^{2+}$ exchange with $Na^{+}$ (11). Alternatively, CGP treatment of mitochondria, by promoting more $Ca^{2+}$ retention in the matrix, could induce mPTP opening and thus decrease RCRs.

To further investigate the role of $Ca^{2+}$ on oxidative phosphorylation, we performed similar experiments using α-ketoglutarate (Fig. 2), another substrate metabolized by a dehydrogenase in which affinity is modulated by $Ca^{2+}$ *in vitro* (14-17). Once again, only low and medium, but not high (Fig. S1B), $Ca^{2+}$ concentrations could be taken up and retained by mitochondria respiring on α-ketoglutarate (Fig. 2A). Using α-ketoglutarate as substrate, medium $Ca^{2+}$ concentrations (22.0 ± 2.4 μM $Ca^{2+}$) increased states 3, 4, and RCR (Fig. 2B-G). Low $Ca^{2+}$ concentrations did not present a significant effect when α-ketoglutarate was used as the substrate. The beneficial effect of $Ca^{2+}$ on mitochondrial oxidative phosphorylation supported by α-ketoglutarate was partially attenuated by inhibition of $Ca^{2+}$ release by NCLX and totally prevented by inhibition of $Ca^{2+}$ entry with RuRed (Fig. 2H), demonstrating again the need for $Ca^{2+}$ entry into the matrix for the stimulatory effect. These results show that the specific "sweet spot" for enhanced electron transport capacity in mitochondria induced by $Ca^{2+}$ varies with the substrate used.

To further investigate substrate-specific effects of $Ca^{2+}$, we performed similar experiments using the complex II substrate succinate in the presence of complex I inhibition with rotenone, to ensure no effect of contaminating or downstream NADH-reducing substrates. With succinate, mitochondria were able to retain a wider range of $Ca^{2+}$ loads (Fig. 3A), so low, medium, and high concentrations were tested for their respiratory effects. Interestingly, using succinate, none of these $Ca^{2+}$ concentrations used led to a significant increase in state 3 or RCR (Fig. 3F,H). A small increase in state 4, in which respiration is not linked to oxidative phosphorylation, was observed with the

medium $Ca^{2+}$ concentration (Fig. 3G), suggesting enhanced proton leak, possibly due to $Ca^{2+}$ cycling or mPTP induction in a subpopulation of the mitochondrial suspension.

Taken together, results using isolated mouse liver mitochondria and various substrates show that a low increase in mitochondrial $Ca^{2+}$ enhances oxidative phosphorylation capacity and efficiency. This positive effect depends on the substrate used and, when present, requires $Ca^{2+}$ entry into the mitochondrial matrix.

### *2.2. Both low and high cytosolic $Ca^{2+}$ impair mitochondrial respiration in cultured hepatocytes*

We investigated next how mitochondrial and cytosolic $Ca^{2+}$ modulate electron transport and oxidative phosphorylation in intact hepatocytes (Fig. 4). Since primary isolated hepatocytes undergo major metabolic alterations during and after isolation (24), defeating the purpose of using a freshly isolated cell, we used AML12 cells, a non-tumoral hepatocyte cell line (25), and thus a more physiological liver cell model. OCRs were measured in plated cells using a Seahorse Extracellular Flux system (26).

To measure the respiratory effects of physiological $Ca^{2+}$ concentrations, we removed increasing amounts of this ion from the cytosol by incubating AML12 cells in complete medium with a cytosolic $Ca^{2+}$ chelator, BAPTA-AM, at different concentrations (Fig. 4 A-C). BAPTA-AM reduced maximal OCR respiration in a dose-dependent manner (Fig. 4C), but no changes were observed in basal respiration (Fig. 4B), which in intact cells corresponds to the respiration necessary to maintain normal levels of oxidative phosphorylation for typical cell function, in addition to the proton leak and non-mitochondrial oxygen consumption (inhibited in each trace by the addition of rotenone plus antimycin A, R/AA). Thus, decreasing physiological cytosolic $Ca^{2+}$ levels hampers maximal electron transfer capacity in hepatocytes, but not sufficiently to decrease ATP-linked respiration under normal (basal) conditions of cell function.

In order to increase physiological intracellular $Ca^{2+}$ levels and study the effects on mitochondrial oxidative phosphorylation, we used a sarco-/endoplasmic reticulum $Ca^{2+}$ ATPase (SERCA) pump inhibitor, thapsigargin (TG), which releases the ion from endoplasmic reticulum (ER) stores. As the ER and mitochondria are closely connected in microdomains called mitochondria-associated ER membranes, this is expected to impact on mitochondrial $Ca^{2+}$ homeostasis. Interestingly, AML12 cells exposed to different concentrations of TG displayed a decrease in basal and maximal respiration (Fig. 4D-F). Taken together, the results in Fig. 4 show that physiological intracellular $Ca^{2+}$

homeostasis is maintained close to the Goldilocks "sweet spot" for oxidative phosphorylation activity, with both increases and decreases in this concentration hampering ideal electron transport function.

### *2.3. $Ca^{2+}$-induced impairment of mitochondrial respiration in hepatocytes is substrate-dependent*

We next speculated if the $Ca^{2+}$ effects on respiration in intact cells could also be substrate-dependent. We used three inhibitors that affect the oxidation of primary substrates that fuel mitochondria: glucose/pyruvate (UK5099), glutamine (BPTES), and long-chain fatty acids (etomoxir). We found that the decrease in basal and maximal respiration was prevented with glucose/pyruvate metabolism inhibition by UK5099 (Fig. 5A,B), showing that the modulation of respiration by $Ca^{2+}$ in intact hepatocytes is dependent on pyruvate oxidation, corroborating data observed in the isolated liver mitochondria (Fig. 1).

### *2.4. Inhibition of mitochondrial $Ca^{2+}$ entry impairs mitochondrial respiration in cultured hepatocytes*

We then questioned if the effects of $Ca^{2+}$ on OCRs in intact cells required $Ca^{2+}$ entry into the matrix, as we found in isolated mitochondria. Inhibition of the MCU or NCLX was promoted in AML12 cells both pharmacologically with RuRed or CGP and by silencing with specific siRNAs. We found that an acute inhibition of the transporters (1 h in the presence if these drugs) did not influence basal respiration (Fig. 6A,B), but MCU inhibition with RuRed led to a tendency toward decreased maximal respiration (Fig. 6A,C). Cells in which NCLX was inhibited by CGP had similar profiles to untreated control cells (Fig. 6A-C).

We then checked how prolonged inhibition of those channels impacted respiration by silencing MCU or NCLX with siRNAs (Fig. S2). Interestingly, we found that overall cytosolic $Ca^{2+}$ levels were similar in these cells, despite the lack of these major mitochondrial $Ca^{2+}$ regulatory pathways (Fig. S3), both under basal conditions and after ER $Ca^{2+}$ depletion due to TG addition. Chronic inhibition of both channels led to a modest tendency toward a decrease in basal respiration (Fig. 6D,E), while MCU knockdown led to a significant decrease in maximal respiration (Fig. 6D,F). This shows that both short and long-term MCU inhibition impact on mitochondrial activity in intact hepatic cells.

### *2.5. $Ca^{2+}$-induced impairment of mitochondrial respiration in hepatocytes occurs secondarily to mPTP opening*

Having uncovered the effects of mitochondrial $Ca^{2+}$ cycling on cellular respiration under physiological conditions, we sought to dissect the reasons for decreased basal respiration induced by $Ca^{2+}$ release from the ER promoted by TG (Fig. 7). Acute MCU inhibition with RuRed (Fig. 7A-D), as well as chronic MCU inhibition with MCU knockdown (Fig. 7E-H) protects mitochondrial respiration against TG-induced decreases, indicating that $Ca^{2+}$ from the ER released by TG is taken up by mitochondria and affects electron transport. In line with this, cytosolic $Ca^{2+}$ chelation with BAPTA-AM also protected from TG-induced decrease of mitochondrial respiration (Fig. 8). $Ca^{2+}$ overload in mitochondria is known to promote the opening of mPTP (18-20), which can decrease OCRs by limiting mitochondrial cytochrome c content and affecting substrate import into the organelle. Thus, we incubated cells with TG in the presence of the mPTP inhibitor cyclosporin A (CsA), which efficiently prevented TG effects (Fig. 8), showing the involvement of mPTP in TG-induced OCR decrease.

## 3. Discussion

Mitochondria are well recognized as a major hub for calcium ($Ca^{2+}$) handling and energy metabolism (1), however, the precise relationship between these two processes under physiologically relevant conditions in the liver was, surprisingly, not studied to date. Instead, small amounts of $Ca^{2+}$ have been shown to increase the affinity of some matrix dehydrogenases, and thus assumed to possibly positively impact on ATP production. This assumption is a tricky one, since $Ca^{2+}$ acts in different ways in mitochondria depending on concentration. Indeed, matrix $Ca^{2+}$ overload is the focus of many studies, and has been shown to promote impairment of mitochondrial function and cell death (27) in a myriad of pathological conditions.

We designed two types of experiments aimed at understanding the effects of $Ca^{2+}$ ions on oxidative phosphorylation in a more global manner, both focused on liver metabolism, as the effects of $Ca^{2+}$ ions on this organ´s rich metabolic activities have, surprisingly, not been dissected to date with respect to mitochondrial electron transport and ATP synthase activity. The first approach involved isolated mitochondria (Figs. 1-3), in which precise concentrations of extramitochondrial $Ca^{2+}$ can be added, and the oxidation of different substrates can be examined while still preserving intact oxidative phosphorylation pathways, thus allowing to establish the impact of $Ca^{2+}$ ions on overall metabolic fluxes.

Our results show that isolated liver mitochondria present enhanced oxidative phosphorylation efficiency promoted by $Ca^{2+}$, in a manner dependent on the substrate used and $Ca^{2+}$ concentrations. Increased respiratory control ratios (RCRs) were achieved with low extramitochondrial $Ca^{2+}$ ($2.4 \pm 0.6$ µM) additions in the presence of the complex I substrates pyruvate plus malate (Fig. 1), and with medium $Ca^{2+}$ ($22.0 \pm 2.4$ µM) in the presence of α-ketoglutarate (Fig. 2). Interestingly, previous reports show that pyruvate dehydrogenase (PDH) and α-ketoglutarate dehydrogenase (α-KGDH) are directly or indirectly activated by $Ca^{2+}$ within the same concentration range (0.1 to 10 µM) in rat mitochondria from heart (30,31), skeletal muscle (32), adipose tissue (33) and liver (34). However, our results suggest that more $Ca^{2+}$ is required to change α-KGDH- versus PDH-supported respiration in mouse liver mitochondria (Figs. 1,2). This confirms that results showing changes in affinities of isolated enzymes cannot be used as predictors on metabolic fluxes in intact organelles; indeed, measured changes in affinity cannot predict metabolic fluxes without considering the concentrations of the substrates/intermediates,

as enzymes activated by $Ca^{2+}$ may already be at their Vmax in the microenvironment of the mitochondrial matrix.

On the other hand, when complex II substrate succinate was used, extramitochondrial $Ca^{2+}$ did not modulate mitochondrial efficiency (Fig. 3). In line with this, recent results (28) show that isolated heart and kidney mitochondria exposed to pyruvate plus malate or α-ketoglutarate plus malate have increased RCRs when in the presence of small increases in $Ca^{2+}$ concentrations (in the nanomolar range), but had decreased RCRs when $Ca^{2+}$ was further augmented. In contrast, $Ca^{2+}$ addition to isolated brain mitochondria energized by pyruvate plus malate leads to reduced RCRs, in a concentration-dependent manner, with no effect on PDH activity (29). These results, overall, show that positive effects of $Ca^{2+}$ on respiration are highly tissue-dependent, and, when present, occur within a tight range of concentrations.

A major concern regarding $Ca^{2+}$ effects presented in the literature is a possible lack of homogeneity in $Ca^{2+}$ concentrations used not only between different studies, but also in replicates within each study. Different $Ca^{2+}$ amounts can be present in distinct isolated mitochondrial preparations, as these carry with them varying quantities of chelators from the isolation buffer. In order to minimize possible confounding results, we found it crucial to determine the amount of $Ca^{2+}$ present after isolation daily and adjust $Ca^{2+}$ added, so it was equal between biological replicates. This may have been a seminal feature which allowed us to uncover activating $Ca^{2+}$ effects, as these were often subtle and concentration-specific. We also exclusively tested on respiration $Ca^{2+}$ concentrations in which we observed no mitochondrial permeability transition pore (mPTP) opening, as indicated by the fact that mitochondrial preparations were able to uptake and retain the ion. Interestingly, the concentrations necessary to induce mPTP are different with distinct substrates, and larger for succinate (Fig. 3) than NADH-linked substrates (Fig. S1), thus allowing us to test more $Ca^{2+}$ concentrations on respiration supported by succinate (with negative results).

But while isolated mitochondrial studies allow the dissection of precise effects of substrates and specific ion concentrations, they do not represent the metabolic state of oxidative phosphorylation in intact cells. Thus, our second approach was to modulate mitochondrial $Ca^{2+}$ levels in the non-tumor AML12 hepatocyte cell line (25). In intact cells, overall $Ca^{2+}$ concentrations are in the 100-150 nM range (Fig. S3), which is much lower than concentrations that activate oxidative phosphorylation in isolated mitochondria, but does not reflect differences in local ion concentrations, such as those

in the $Ca^{2+}$-rich mitochondrial-endoplasmic reticulum (ER) contact sites, where $Ca^{2+}$ concentration may be up to 10 times higher than in the bulk cytosol (30-32).

We found that the $Ca^{2+}$ concentrations in mitochondria *in situ* are both necessary and sufficient to enhance electron transport capacity through various different approaches. First, chelation of intracellular $Ca^{2+}$ with BAPTA-AM decreased maximal OCR (Fig. 4C), without affecting mitochondrial membrane integrity, as indicated by the lack of change in oligomycin-insensitive respiration (Fig. 4A). Second, inhibition of mitochondrial $Ca^{2+}$ uptake with ruthenium red (RuRed) or by silencing the mitochondrial $Ca^{2+}$ uniporter (MCU) (Fig. 6) also decreased maximal electron transport capacity in intact cells, indicating that ideal respiratory chain function requires both the presence of physiological levels of cytosolic $Ca^{2+}$ and its uptake by mitochondria. Our results are compatible with data showing that genetic manipulation of MCU and consequent impairment of mitochondrial $Ca^{2+}$ uptake disrupts oxidative phosphorylation and lowers cellular ATP in HeLa cells (39). Similarly, mitochondria from a liver-specific MCU knockout mouse model also had inhibition of mitochondrial $Ca^{2+}$ uptake and reduced oxidative phosphorylation (40).

Conversely, we increased cytosolic levels to ~200 nM by adding thapsigargin (TG) to induce ER $Ca^{2+}$ depletion (Fig. S3, Fig. 4). TG is a well-known sarco-/endoplasmic reticulum $Ca^{2+}$ ATPase (SERCA) pump inhibitor. SERCA is localized at mitochondrial-associated ER membrane microdomains where the ER and mitochondria are in close proximity, allowing for communication between both organelles and $Ca^{2+}$ exchange (33,34). We also increased mitochondrial $Ca^{2+}$ by inhibiting the NCLX extrusion pathway with CGP or silencing. Both strategies to increase $Ca^{2+}$ in intact cells lead to lower maximal respiratory rates (Figs. 4 and 6), indicating that physiological $Ca^{2+}$ levels in mitochondria are at the ideal level to maximize electron transport, with both decreases and increases leading to lower efficiency in this process. These results are in line with the finding that constitutive IP3R-mediated ER $Ca^{2+}$ release to mitochondria is essential for efficient mitochondrial respiration and maintenance of normal cell bioenergetics (35). On the other hand, cells expressing a truncated variant of SERCA-1 with increased ER-mitochondria contact sites and increased $Ca^{2+}$ transfer from the ER to mitochondria show signs of mitochondrial dysfunction due to $Ca^{2+}$ overload (36).

Maximal OCR limitation observed under these conditions of $Ca^{2+}$ overload in intact cells is due to uptake of the ion into the mitochondrial matrix, as it is inhibited by BAPTA-AM, MCU silencing or pharmacological inhibition (Figs. 7 and 8). Excess

mitochondrial $Ca^{2+}$ is known to lead to mPTP opening and consequent dissipation of the mitochondrial membrane potential, mitochondrial swelling and rupture, culminating in cell death (18-20). Since the decrease in OCR observed under our conditions of mitochondrial $Ca^{2+}$ overload was prevented by mPTP inhibitor cyclosporin A (CsA, Fig. 8), it is attributable to this form of mitochondrial inner membrane permeabilization.

While it may seem instinctively obvious that physiological resting mitochondrial $Ca^{2+}$ levels would be at ideal quantities to activate maximum electron transport achievable, but not generate mitochondrial damage, it should be noted that not all intracellular signaling situations operate physiologically at maximum capacity. Perhaps the best example in this context is mitochondrial electron transfer itself, which is typically lower under basal conditions than maximum capacity uncovered when in the presence of uncoupler (see Figs. 4-8). Indeed, the difference between basal OCR and maximal achievable electron transport, known as reserve capacity, is thought to be important in resistance toward stress; a manner to allow fast increments in ATP synthesis when necessary (37). On the other hand, our results in hepatocytes show clearly that physiological $Ca^{2+}$ levels in mitochondria are specifically those that maintain the highest maximal OCR without promoting mPTP. Overall, we demonstrate that hepatocytes maintain cellular and mitochondrial $Ca^{2+}$ concentrations in strictly controlled ranges, maximizing electron transport capacity by promoting the Goldilocks $Ca^{2+}$ “sweet spot” for oxidative phosphorylation activity: neither too much, nor too little, but just right.

## 4. Experimental procedures

### *4.1. Reagents*

Culture medium (DMEM/F-12), fetal bovine serum (FBS), insulin-transferrin-selenium (ITS), $Ca^{2+}$ Green 5N and Pierce BCA protein assay kit were from Thermo Fischer Scientific (Waltham, MA, USA); thapsigargin, BAPTA-AM, CGP37157, ruthenium red, UK5099, BPTES, etomoxir and RIPA buffer were from Sigma-Aldrich (St. Louis, MO, USA); lipofectamine RNAiMAX, Trizol reagent and Fura-2 AM were from Invitrogen (Waltham, MA, USA); Bradford was from Bio-Rad Laboratories (Hercules, CA, USA); siRNAs against MCU (ID s103465), NCLX (ID s100747) or negative control (#4390844) were from Ambion Inc. (Austin, TX, USA); anti-MCU (#14997S) was from Cell Signaling (Danvers, MA, USA); anti-β-actin (#ab8226) was from Abcam (Cambridge, UK); fluorescent secondary antibodies (goat anti-mouse #926-68070 and goat anti-rabbit #926-68071) were from Licor (Lincoln, NE, USA).

### *4.2. Animals*

C57BL/6NTac male mice were bred and housed in the animal facility of the Faculty of Pharmaceutical Sciences and Chemistry Institute of the University of São Paulo, devoid of murine pathogens. Animals were maintained in collective cages (max 4/cage) at controlled temperatures (23°C) in a 12–12 h light/dark cycle with free access to food/water. We used 10–12-week-old mice. All procedures were conducted in accordance with the Ethical Principles of Animal Manipulation of the local animal ethics committee, under protocol CEUA-IQ/USP 196/2021.

### *4.3. Isolation of liver mitochondria*

After deep anesthesia (4% isoflurane) followed by cervical dislocation, the abdomen was dissected and the liver was removed. Mitochondria were isolated by differential centrifugation. All steps were carried out at 4°C, over ice. Briefly, the liver was chopped into small pieces, suspended in isolation buffer (250 mM sucrose, 10 mM HEPES, 1 mM EGTA, 1 mM EDTA, 1 mg/ml BSA, pH 7.2) and manually homogenized using a Potter-Elvehjem tissue grinder. To remove blood from the mixture, it was centrifuged twice (800 g, 4ºC, 4 min) and the pellet was discharged. The supernatant was further centrifuged at 9,000 g, 4ºC for 10 min. The pellet was resuspended in resuspension buffer (300 mM sucrose, 10 mM HEPES and 2 mM EGTA, pH 7.2) and centrifuged again (9,000 g, 4ºC,

10 min). The pellet was resuspended in 125 µL of resuspension buffer and total protein was quantified using the Bradford method.

### *4.4. Oxygen consumption by isolated liver mitochondria*

Oxygen consumption was measured using a high-resolution Oxygraph-2k (O2k) respirometer (Oroboros Instruments, Innsbruck, Austria). Mitochondria (600 µg protein for pyruvate/malate and α-ketoglutarate; 200 µg protein for succinate/rotenone) were incubated in 2 mL of experimental buffer (125 mM sucrose, 65 mM KCl, 10 mM HEPES, 2 mM $MgCl_2$, 2 mM $KH_2PO_4$ and 0.1 mg/ml BSA) containing 100 µM EGTA and different substrates (1 mM pyruvate + 1 mM malate, 1 mM α-ketoglutarate or 1 mM succinate + 1 µM rotenone) and/or inhibitors (10 µM ruthenium red or 10 µM CGP37157) at 37ºC with continuous stirring (700 rpm). After basal respiration was measured, $CaCl_2$ was injected at different concentrations, as indicated. After reaching a steady state (as indicated by $Ca^{2+}$ uptake measurements), state 3 respiration was measured by adding 1 mM ADP, followed by addition of 1 µM oligomycin (State 4), and 0.5 µM CCCP (state 3u). Respiratory control ratios (RCR) were calculated as State 3/State 4.

### *4.5. Calcium ($Ca^{2+}$) uptake assays*

$Ca^{2+}$ measurement assays were performed simultaneously to oxygen consumption measurements, in order to determine the approximate free extramitochondrial $Ca^{2+}$ concentration and to monitor $Ca^{2+}$ levels over time, as done in (38), as well as to monitor mPTP opening. Mitochondria (600 µg protein for pyruvate/malate and α-ketoglutarate; 200 µg protein for succinate/rotenone) were incubated in 2 mL of the same experimental buffer used in the oxygen consumption assay, containing 0.1 µM Calcium Green 5N, 100 µM EGTA and different substrates and inhibitors, as indicated. Calcium Green fluorescence was measured at $\lambda_{ex}$ = 506 nm and $\lambda_{em}$ = 532 nm, using a F4500 and a F2500 Hitachi Fluorimeters at 37ºC with continuous stirring. After a 100 s baseline interval, a $CaCl_2$ solution was added to achieve the target $Ca^{2+}$ concentrations (low, medium and high, as indicated), and fluorescence was monitored for 20 min. Each trace was followed by three 10 µM $Ca^{2+}$, three 1 mM $Ca^{2+}$, and three 3 mM EGTA additions, to allow the estimation of the Calcium Green 5N experimental Kd, and maximal (Fmax) and minimal (Fmin) fluorescence, respectively. Absolute fluorescence values (F) were calibrated into $[Ca^{2+}]$ through the formula $[Ca^{2+}] = Kd.(F - Fmin)/(Fmax - F)$.

### *4.6. AML-12 cell cultures*

The hepatocyte AML-12 cell line was maintained in DMEM/F-12 medium supplemented with 10% (v/v) FBS, a mixture of insulin, transferrin, and selenium (ITS; Collaborative Research), 1% antibiotics (100 U/ml penicillin, 0.1 mg/ml streptomycin), pH 7.4, at 37°C in a humidified atmosphere of 5% $CO_2$.

### *4.7. Small interfering RNA (siRNA) transfection*

AML-12 cells were transfected with siRNAs against MCU, NCLX or scramble RNA as a negative control (Ambion Inc.), using Lipofectamine RNAiMAX and a reverse transfection protocol. Briefly, lipofectamine and siRNAs were diluted in Opti-MEM medium and were added to the cell suspension at a final concentration of 20 nM. Cells were kept overnight at 37°C in DMEM/F-12 containing ITS, without antibiotics. After transfection, the medium was replaced by complete medium. 48 h after transfection, cells were seeded for experiments and let for additional 24 h.

### *4.8. RT-qPCR*

After transfections with siRNAs, AML-12 cells were collected with Trizol™ Reagent and RNA was isolated following the manufacturer's instructions. Total RNA was quantified using a NanoDrop® spectrophotometer and cDNA synthesis was performed using the High-Capacity cDNA Reverse Transcription Kit. qPCR reactions were performed using the Platinum® SYBR® Green qPCR SuperMix-UDG along with specific primers for *Mcu* (FW 5'-ACTCACCAGATGGCGTTCG-3'; RV 5'-CATGGCTTAGGAGGTCTCTCTT-3'), *Nclx* (FW 5'-TGTCACCTTCCTGGCCTTTG-3'; RV 5'-CACCCCTGCACCAAACAGA-3'), *Hmbs* (FW 5'-CAGCTACAGAGA AAGTTCCCC-3'; RV 5'-AGGACGATGGCACTGAATTC-3') and *B2m* (FW 5'-CTGGTCTTTCTATATCCTGGCTC-3'; RV 5'-TGCTTGATCACATGTCTCGATC-3') genes. Amplification data was analyzed by the $2^{(-\Delta\Delta Ct)}$ method using the mean of *Hmbs* and *B2m* Ct values as housekeeping. The housekeeping choice was based on the stability value of the gene or combination of genes calculated by the NormFinder Software (39).

### *4.9. Western blot*

In order to validate MCU silencing, we performed a western blot analysis of MCU levels in transfected AML-12 cells. Briefly, cells were lysed in RIPA buffer containing protease and phosphatase inhibitor cocktails, and total protein levels were quantified using Pierce

BCA Protein Assay kit. Lysates were prepared in sample buffer (2% SDS, 10% Glycerol, 0.062 M Tris pH 6.8, 0.002% Bromophenol Blue, 5% 2-mercaptoethanol), loaded onto SDS-PAGE gels and electrotransfered to PVDF membranes. Membranes were blocked with 5% BSA in TTBS (20 mM Tris pH 7.5, 150 mM NaCl and 0.1% Tween 20) for 1 hour at room temperature before overnight incubation with MCU (1:1,000) and β-actin (1:5,000) primary antibodies at 4°C. Fluorescent secondary antibodies (1:15,000) were incubated for 1 hour at room temperature prior to fluorescence detection using a ChemiDoc™ Imaging System (Bio-Rad). Quantification of band densitometry was performed using the FIJI ImageJ software.

### *4.10. Cytosolic $Ca^{2+}$ measurements*

After MCU or NCLX silencing, AML-12 cells were seeded at 1.5 x $10^6$ cells in 4 mL complete medium in 60 mm cell culture dishes. After 24 h, cells were loaded with 5 µM Fura-2 AM for 1 h at 37ºC. After the loading period, cells were tripsinized and suspended in Krebs-Henseleit buffer without $CaCl_2$ (115 mM NaCl, 24 mM $NaHCO_3$, 5 mM KCl, 1 mM $MgSO_4$, 1.2 mM $KH_2PO_4$). 1 x $10^6$ cells (final volume: 2 mL) were checked for basal cytosolic $Ca^{2+}$ levels and after ER $Ca^{2+}$ depletion with thapsigargin using a F4500 Hitachi Fluorimeter at 37ºC with continuous stirring. Fluorescence was measured at excitation 340/380 nm and emission 505 nm. Each trace was followed by 4% Triton X-100 (50 µL) and 60 mM EGTA (150 µL) additions, to allow the estimation of maximal ($R_{max}$) and minimal ($R_{min}$) fluorescence ratio, respectively. Intracellular $Ca^{2+}$ concentrations, $[Ca^{2+}]_i$, were calculated as described in (40) through the formula $[Ca^{2+}]_i$ (nM) = $K_d \times [(R - R_{min}) / R_{max} - R)] \times Sfb$, where the $K_d$ for $Ca^{2+}$ binding to Fura-2 at 37°C = 225 nM and Sfb is the ratio of baseline fluorescence at 380 nm.

### *4.11. Oxygen consumption in intact AML-12 cells*

Cells were seeded at 30,000 cells per well in 100 µL DMEM/F-12 medium (with 10% FBS, 1% P/S, ITS) on Agilent Seahorse XF24 cell culture microplates and allowed to adhere overnight. Oxygen consumption was measured using a Seahorse Extracellular Flux Analyzer (Agilent Technologies, Santa Clara, CA, EUA). For that, cells were washed thrice with 500 µL DMEM/F-12 containing 1% P/S and 5 mM HEPES. Media did not contain bicarbonate nor FBS. Cells were kept for 1 h in a humidified incubator at 37ºC without $CO_2$, in the absence or presence of different additions (BAPTA-AM, 10 µM ruthenium red, 10 µM CGP37157), as indicated. After incubation, plates were placed in

the equipment and oxygen consumption rates (OCR) were measured under basal conditions, followed by different injections: a) thapsigargin (TG, final concentration: 2 µM) or same volume of DMSO in control wells; b) oligomycin (final concentration: 1 µM); c) CCCP (final concentration: 5 µM); d) antimycin and rotenone (R/AA, final concentration: 1 µM each). Cell-free wells were incubated with same medium for background correction, calculated by subtracting changes observed from the experiments in the presence of cells. OCR values obtained were normalized per amount of total protein in each well. For that, at the end of each experiment, the medium was removed, cells were PBS-washed, lysed with RIPA buffer, and total protein was quantified using the BCA Pierce protocol.

### *4.12. Substrate oxidation test*

Different substrate oxidation effects on respiration were evaluated using inhibitors for three primary substrates that fuel mitochondria: glucose/pyruvate (12 µM UK5099), glutamine (8 µM BPTES) and long-chain fatty acids (14 µM Etomoxir). Oxygen consumption was measured in AML-12 cells in suspension using a high-resolution O2k respirometer (Oroboros Instruments). 1 x $10^6$ cells were incubated in 2 mL of the same medium used in Seahorse experiments in the absence or presence of 2 µM thapsigargin and/or inhibitors, at 37ºC with continuous stirring (400 rpm). After basal respiration, 1 µM oligomycin was injected, followed by 5 µM CCCP, to calculate maximal respiration.

### *4.13. Statistical analysis*

Statistical analysis was carried out using GraphPad Prism 8 Software for at least three independent experiments (biological replicates). Student's t test was used to compare differences between treated and untreated conditions and One-way ANOVA followed by Sidak was used to compare multiple conditions, with confidence levels set to $p < 0.05$. Data shown in scatter graphs are individual biological replicates, averages and standard deviations.

**Figure legends**

**Figure 1. $Ca^{2+}$ uptake increases liver mitochondrial oxidative phosphorylation supported by pyruvate and malate.** Isolated mouse liver mitochondria (600 µg) were incubated with 1 mM pyruvate + 1 mM malate. **A)** Representative $Ca^{2+}$ uptake curves measured using $Ca^{2+}$ Green N to measure extramitochondrial $Ca^{2+}$, in the presence of low $Ca^{2+}$ (2.4 ± 0.6 µM, black line) and medium $Ca^{2+}$ (22.0 ± 2.4 µM, blue line) concentrations. **B-D)** Representative $O_2$ consumption rate (OCR) traces using a high-resolution Oxygraph-2k (O2k) respirometer in response to no $Ca^{2+}$ **(B)**, low $Ca^{2+}$ **(C)** and medium $Ca^{2+}$ **(D)** additions, followed by injection of 1 mM ADP, 1 µM oligomycin and 0.5 µM CCCP. **E)** State 3, after ADP injection. **F)** State 4, after oligomycin injection. **G)** Respiratory control ratios (RCR, state 3 / state 4). **H)** RCR in the presence of low $Ca^{2+}$ and 10 µM CGP37157 (CGP) or 10 µM ruthenium red (RuRed). N = 4 independent experiments. *p<0.05 versus control using One-way ANOVA followed by Sidak.

**Figure 2. $Ca^{2+}$ uptake increases liver mitochondrial oxidative phosphorylation supported by α-ketoglutarate.** Isolated mouse liver mitochondria (600 µg) were energized with 1 mM α-ketoglutarate. **A)** Representative $Ca^{2+}$ uptake curves in the presence of low $Ca^{2+}$ (2.4 ± 0.6 µM, black line) and medium $Ca^{2+}$ (22.0 ± 2.4 µM, blue lines). **B-D)** Representative OCR traces with zero $Ca^{2+}$ **(B)**, low $Ca^{2+}$ **(C)** and medium $Ca^{2+}$ **(D)**, followed by injection of 1 mM ADP, 1 µM oligomycin and 0.5 µM CCCP. **E)** State 3, after ADP injection. **F)** State 4, after oligomycin injection. Respiratory control ratio (RCR, state 3 / state 4). **H)** RCR in the presence of medium $Ca^{2+}$ and CGP or RuRed. N = 4 independent experiments. *p<0.05 and **p<0.01 versus control using One-way ANOVA followed by Sidak.

**Figure 3. $Ca^{2+}$ uptake does not increase liver mitochondrial oxidative phosphorylation supported by succinate.** Isolated mouse liver mitochondria (200 µg) were energized with 1 mM succinate in the presence of 1 µM rotenone. **A)** Representative $Ca^{2+}$ uptake curves in the presence of low $Ca^{2+}$ (2.4 ± 0.6 µM, black line), medium $Ca^{2+}$ (22.0 ± 2.4 µM, blue line) and high $Ca^{2+}$ (52.9 ± 2.5 µM, purple line). **B-E)** Representative OCR traces in response to no $Ca^{2+}$ **(B)**, low $Ca^{2+}$ **(C)**, medium $Ca^{2+}$ **(D)**, and high $Ca^{2+}$ **(E)**, followed by injection of 1 mM ADP, 1 µM oligomycin and 0.5 µM CCCP. **F)** State 3, after ADP injection. **G)** State 4, after oligomycin injection. **H)** Respiratory control

ratios (RCR, state 3 / state 4). N = 4 independent experiments. *p<0.01 versus control using One-way ANOVA followed by Sidak.

**Figure 4. Depletion of intracellular $Ca^{2+}$ stores in hepatocytes limits maximal mitochondrial respiration. A-C)** AML12 cells were pre-incubated for 1 h in the absence (control) or presence of a cytosolic $Ca^{2+}$ chelator, BAPTA-AM, at different concentrations (5 - 20 µM, as shown), and OCRs was measured using a Seahorse Extracellular Flux Analyzer. **C-E)** OCRs was measured under basal conditions, followed by the injection of DMSO (diluent) or thapsigargin (TG, 0.2, 0.5 or 2 µM as indicated). Oligomycin (oligo, 1 µM), CCCP (5 µM) and rotenone + antimycin (R/AA, 1 µM each) were added to all traces as indicated. Results are expressed as representative traces **(A, D)** or means ± SEM (B, C, E, F) of 5 independent biological experiments. *p<0.05 and ***p<0.001 versus control using One-way ANOVA followed by Sidak.

**Figure 5. Intracellular $Ca^{2+}$ modulates mainly mitochondrial pyruvate oxidation.** AML12 cells were incubated in the absence (CT) or presence of 2 µM thapsigargin (TG) and inhibitors (12 µM UK5099, 8 µM BPTES or 14 µM Etomoxir). OCRs were measured under basal conditions, followed by injection of oligomycin (oligo, 1 µM) and CCCP (5 µM), to induce maximal respiration. **A)** Quantification of basal respiration. **B)** Quantification of maximal respiration. Results are expressed as means ± SEM of 4 independent experiments. *p<0.05 versus respective untreated control using Student's t-test.

**Figure 6. Mitochondrial $Ca^{2+}$ uptake increases maximal, but not basal, respiration in intact hepatocytes. A-C)** Cells were incubated for 1 h in the absence (control) or presence of 10 µM of RuRed or CGP. **D-F)** AML12 with siRNAs against MCU (siMCU) or NCLX (siNCLX) or a negative control (siCT). **A,D)** OCRs were measured using a Seahorse Extracellular Flux Analyzer; oligomycin (oligo, 1 µM), CCCP (5 µM), and rotenone + antimycin (R/AA, 1 µM each) were added where indicated. **B,E)** Quantification of basal respiration. **C,F)** Quantification of maximal respiration. Results are expressed as means ± SEM of 3–4 independent experiments. *p<0.05 versus control using Student's t-test.

**Figure 7. High intracellular $Ca^{2+}$ limits maximal respiration in a manner dependent on mitochondrial $Ca^{2+}$ uptake. A-D)** Cells were incubated for 1 h in the absence (CT) or presence of 10 µM of RuRed or CGP. **E-H)** Cells treated with specific siRNAs against the MCU (siMCU) or NCLX (siNCLX) or a negative control (siCT). OCRs were measured in a Seahorse Extracellular Flux Analyzer under basal conditions, followed by injection of DMSO (diluent) or 2 µM thapsigargin (TG), oligomycin (oligo, 1 µM), CCCP (5 µM) and rotenone + antimycin (R/AA, 1 µM each). **C, D)** Quantifications of basal and **(G,H)** maximal respiration. Results are expressed as mean ± SEM of 3–4 independent experiments. *p<0.05 and ***p<0.001 versus respective control using Student's t-test.

**Figure 8. Respiratory inhibition promoted by excess $Ca^{2+}$ is due to mPTP. A-C)** OCRs were under basal conditions followed by injection of i) DMSO (diluent) or 2 µM thapsigargin (TG) or 10 µM cyclosporin A (CsA) or TG + CsA, ii) oligomycin (oligo, 1 µM), iii) CCCP (5 µM) and iv) rotenone + antimycin (R/AA, 1 µM each). **B)** Cells were pre-incubated for 1 h in the absence or presence of a cytosolic $Ca^{2+}$ chelator, 10 µM BAPTA-AM (BAPTA), before OCR measurements. **D)** Quantification of basal respiration. **E)** Quantification of maximal respiration. Results are expressed as mean ± SEM of 4 independent experiments. *p<0.05 and **p<0.01 versus respective control using Student's t-test.

**Figure S1. High $Ca^{2+}$ concentration leads to mPTP opening in liver mitochondria in the presence of pyruvate plus malate or α-ketoglutarate. A,B)** Representative $Ca^{2+}$ uptake curves measured using $Ca^{2+}$ Green N, in the presence of high $Ca^{2+}$ concentrations. Isolated mouse liver mitochondria (600 µg) were incubated with 1 mM pyruvate plus 1 mM malate (pyr + mal, **A**) or 1 mM α-ketoglutarate (α-KG, **B**). Calcium uptake by mitochondria leads to a decrease in fluorescence over the first few minutes, which was not maintained over time, indicating lack of mitochondrial ability to maintain high $Ca^{2+}$ uptake over the experimental time period.

**Figure S2. MCU and NCLX silencing. A)** NCLX mRNA levels after 48, 72 and 96 h of transfection with specific siRNA against NCLX (siNCLX) or a negative control (siCT). **B)** MCU mRNA levels after 48 and 72 h of transfection with specific siRNA against MCU (siMCU) or a negative control (siCT). **C)** Representative western blots of MCU and β-actin (internal control) after 72 h of transfection with specific siRNA against

MCU (siMCU) or a negative control (siCT). **D)** Densitometric analysis of the Western blots. *p<0.05 and ****p<0.0001 versus respective control using Student's t-test.

**Figure S3. Cytosolic $Ca^{2+}$ levels in siMCU or siNCLX cells are preserved. A)** Typical cytosolic $Ca^{2+}$ measurements performed using Fura-2. **B)** Quantification under basal conditions. **C)** Quantification of the peak after the addition of thapsigargin.

## Data availability

All data are contained within the manuscript and supporting information.


## Acknowledgements

This work was supported mainly by the *Fundação de Amparo à Pesquisa do Estado de São Paulo* (FAPESP) under grant numbers 13/07937-8, 17/14713-0, 19/18402-4, and 21/02481-2, as well as the *Conselho Nacional de Desenvolvimento Científico e Tecnológico* (CNPq) and *Coordenação de Aperfeiçoamento de Pessoal de Nível Superior* (CAPES) line 001. We acknowledge Silvânia M. P. Neves and her animal facility crew for exceptional expert animal care.


## Conflict of interest

The authors declare that they have no conflicts of interest.

## Author contributions

E.A.V.-B. and A.J.K. are responsible for concept and design; E.A.V.-B., J.V.C.-C., V.M.R. and C.C.C.S. performed experiments; E.A.V.-B., J.V.C.-C. and A.J.K. interpreted the data and discussed the results; E.A.V.-B. and A.J.K. prepared figures and drafted the manuscript; all authors revised and approved final version of manuscript.

**REFFERENCES**


1. Giorgi, C., Marchi, S., and Pinton, P. (2018) The machineries, regulation and cellular functions of mitochondrial calcium. *Nat Rev Mol Cell Biol* **19**, 713-730

2. Deluca, H. F., and Engstrom, G. W. (1961) Calcium uptake by rat kidney mitochondria. *Proc Natl Acad Sci U S A* **47**, 1744-1750

3. Vasington, F. D., and Murphy, J. V. (1962) Ca ion uptake by rat kidney mitochondria and its dependence on respiration and phosphorylation. *J Biol Chem* **237**, 2670-2677

4. Budd, S. L., and Nicholls, D. G. (1996) A reevaluation of the role of mitochondria in neuronal $Ca^{2+}$ homeostasis. *J Neurochem* **66**, 403-411

5. Hartmann, J., and Verkhratsky, A. (1998) Relations between intracellular $Ca^{2+}$ stores and store-operated $Ca^{2+}$ entry in primary cultured human glioblastoma cells. *J Physiol* **513 ( Pt 2)**, 411-424

6. Williams, G. S., Boyman, L., Chikando, A. C., Khairallah, R. J., and Lederer, W. J. (2013) Mitochondrial calcium uptake. *Proc Natl Acad Sci U S A* **110**, 10479-10486

7. Naon, D., and Scorrano, L. (2014) At the right distance: ER-mitochondria juxtaposition in cell life and death. *Biochim Biophys Acta* **1843**, 2184-2194

8. Kirichok, Y., Krapivinsky, G., and Clapham, D. E. (2004) The mitochondrial calcium uniporter is a highly selective ion channel. *Nature* **427**, 360-364

9. Baughman, J. M., Perocchi, F., Girgis, H. S., Plovanich, M., Belcher-Timme, C. A., Sancak, Y., Bao, X. R., Strittmatter, L., Goldberger, O., Bogorad, R. L., Koteliansky, V., and Mootha, V. K. (2011) Integrative genomics identifies MCU as an essential component of the mitochondrial calcium uniporter. *Nature* **476**, 341-345

10. De Stefani, D., Raffaello, A., Teardo, E., Szabò, I., and Rizzuto, R. (2011) A forty-kilodalton protein of the inner membrane is the mitochondrial calcium uniporter. *Nature* **476**, 336-340

11. Palty, R., Silverman, W. F., Hershfinkel, M., Caporale, T., Sensi, S. L., Parnis, J., Nolte, C., Fishman, D., Shoshan-Barmatz, V., Herrmann, S., Khananshvili, D., and Sekler, I. (2010) NCLX is an essential component of mitochondrial $Na^{+}/Ca^{2+}$ exchange. *Proc Natl Acad Sci U S A* **107**, 436-441

12. [preprint] Austin, S., Mekis, R., Mohammed, S. E. M., Scalise, M., Pfeiffer, C., Galluccio, M., Borovec, T., Parapatics, K., Vitko, D., Dinhopl, N., Bennett, K. L., Indiveri, C., and Nowikovsky, K. (2021) MICS1 is the $Ca^{2+}/H^{+}$ antiporter 1 of mammalian mitochondria. BioRxiv. 10.1101/2021.11.11.468204v1

13. [preprint] Patron, M., Tarasenko, D., Nolte, H., Ghosh, M., Ohba, Y., Lasarzewski, Y., Ahmadi, Z. A., Cabrera-Orefice, A., Eyiama, A., Kellermann, T., Rugarli, E. I., Brandt, U., Meinecke, M., and Langer, T. (2021) Regulation of mitochondrial proteostasis by the proton gradient. BioRxiv. 10.1101/2021.12.12.470907

14. Denton, R. M., and McCormack, J. G. (1985) $Ca^{2+}$ transport by mammalian mitochondria and its role in hormone action. *Am J Physiol* **249**, E543-554

15. Hansford, R. G. (1985) Relation between mitochondrial calcium transport and control of energy metabolism. *Rev Physiol Biochem Pharmacol* **102**, 1-72

16. Rossi, A., Pizzo, P., and Filadi, R. (2019) Calcium, mitochondria and cell metabolism: A functional triangle in bioenergetics. *Biochim Biophys Acta Mol Cell Res* **1866**, 1068-1078

17. Denton, R. M. (2009) Regulation of mitochondrial dehydrogenases by calcium ions. *Biochim Biophys Acta* **1787**, 1309-1316

18. Haworth, R. A., and Hunter, D. R. (1979) The $Ca^{2+}$-induced membrane transition in mitochondria. II. Nature of the $Ca^{2+}$ trigger site. *Arch Biochem Biophys* **195**, 460-467

19. Jia, K., and Du, H. (2021) Mitochondrial permeability transition: a pore intertwines brain aging and alzheimer's disease. *Cells* **10** (3), 649

20. Modesti, L., Danese, A., Angela Maria Vitto, V., Ramaccini, D., Aguiari, G., Gafà, R., Lanza, G., Giorgi, C., and Pinton, P. (2021) Mitochondrial $Ca^{2+}$ signaling in health, disease and therapy. *Cells* **10** (6), 1317

21. Bravo-Sagua, R., Parra, V., López-Crisosto, C., Díaz, P., Quest, A. F., and Lavandero, S. (2017) Calcium transport and signaling in mitochondria. *Compr Physiol* **7**, 623-634

22. Filadi, R., and Greotti, E. (2021) The yin and yang of mitochondrial $Ca^{2+}$ signaling in cell physiology and pathology. *Cell Calcium* **93**, 102321

23. Brand, M. D., and Nicholls, D. G. (2011) Assessing mitochondrial dysfunction in cells. *Biochem J* **435**, 297-312

24. Cassim, S., Raymond, V. A., Lapierre, P., and Bilodeau, M. (2017) From in vivo to in vitro: major metabolic alterations take place in hepatocytes during and following isolation. *PLoS One* **12**, e0190366

25. Wu, J. C., Merlino, G., and Fausto, N. (1994) Establishment and characterization of differentiated, nontransformed hepatocyte cell lines derived from mice transgenic for transforming growth factor alpha. *Proc Natl Acad Sci U S A* **91**, 674-678

26. Ferrick, D. A., Neilson, A., and Beeson, C. (2008) Advances in measuring cellular bioenergetics using extracellular flux. *Drug Discov Today* **13**, 268-274

27. Duchen, M. R., Verkhratsky, A., and Muallem, S. (2008) Mitochondria and calcium in health and disease. *Cell Calcium* **44**, 1-5

28. Zhang, X., Tomar, N., Kandel, S. M., Audi, S. H., Cowley, A. W., and Dash, R. K. (2021) Substrate- and calcium-dependent differential regulation of mitochondrial oxidative phosphorylation and energy production in the heart and kidney. *Cells* **11** (1), 131

29. Pandya, J. D., Nukala, V. N., and Sullivan, P. G. (2013) Concentration dependent effect of calcium on brain mitochondrial bioenergetics and oxidative stress parameters. *Front Neuroenergetics* **5**, 10

30. Tubbs, E., and Rieusset, J. (2017) Metabolic signaling functions of ER-mitochondria contact sites: role in metabolic diseases. *J Mol Endocrinol* **58**, R87-R106

31. Rizzuto, R., and Pozzan, T. (2006) Microdomains of intracellular $Ca^{2+}$: molecular determinants and functional consequences. *Physiol Rev* **86**, 369-408

32. Cremer, T., Neefjes, J., and Berlin, I. (2020) The journey of $Ca^{2+}$ through the cell – pulsing through the network of ER membrane contact sites. *J Cell Sci* **133**

33. Lee, S., and Min, K. T. (2018) The interface between ER and mitochondria: molecular compositions and functions. *Mol Cells* **41**, 1000-1007

34. Csordás, G., Weaver, D., and Hajnóczky, G. (2018) Endoplasmic reticulum-mitochondrial contactology: structure and signaling functions. *Trends Cell Biol* **28**, 523-540

35. Cárdenas, C., Miller, R. A., Smith, I., Bui, T., Molgó, J., Müller, M., Vais, H., Cheung, K. H., Yang, J., Parker, I., Thompson, C. B., Birnbaum, M. J., Hallows, K. R., and Foskett, J. K. (2010) Essential regulation of cell bioenergetics by constitutive InsP3 receptor $Ca^{2+}$ transfer to mitochondria. *Cell* **142**, 270-283

36. Chami, M., Oulès, B., Szabadkai, G., Tacine, R., Rizzuto, R., and Paterlini-Bréchot, P. (2008) Role of SERCA1 truncated isoform in the proapoptotic calcium transfer from ER to mitochondria during ER stress. *Mol Cell* **32**, 641-651

37. Hill, B. G., Benavides, G. A., Lancaster, J. R., Ballinger, S., Dell'Italia, L., Jianhua, Z., and Darley-Usmar, V. M. (2012) Integration of cellular bioenergetics with mitochondrial quality control and autophagy. *Biol Chem* **393**, 1485-1512

38. Kowaltowski, A. J., Menezes-Filho, S. L., Assali, E. A., Gonçalves, I. G., Cabral-Costa, J. V., Abreu, P., Miller, N., Nolasco, P., Laurindo, F. R. M., Bruni-Cardoso, A., and Shirihai, O. S. (2019) Mitochondrial morphology regulates organellar $Ca^{2+}$ uptake and changes cellular $Ca^{2+}$ homeostasis. *FASEB J* **33**, 13176-13188

39. Andersen, C. L., Jensen, J. L., and Ørntoft, T. F. (2004) Normalization of real-time quantitative reverse transcription-PCR data: a model-based variance estimation approach to identify genes suited for normalization, applied to bladder and colon cancer data sets. *Cancer Res* **64**, 5245-5250

40. Patel, A., Hirst, R. A., Harrison, C., Hirota, K., and Lambert, D. G. (2013) Measurement of $[Ca^{2+}]i$ in whole cell suspensions using Fura-2. *Methods Mol Biol* **937**, 37-47

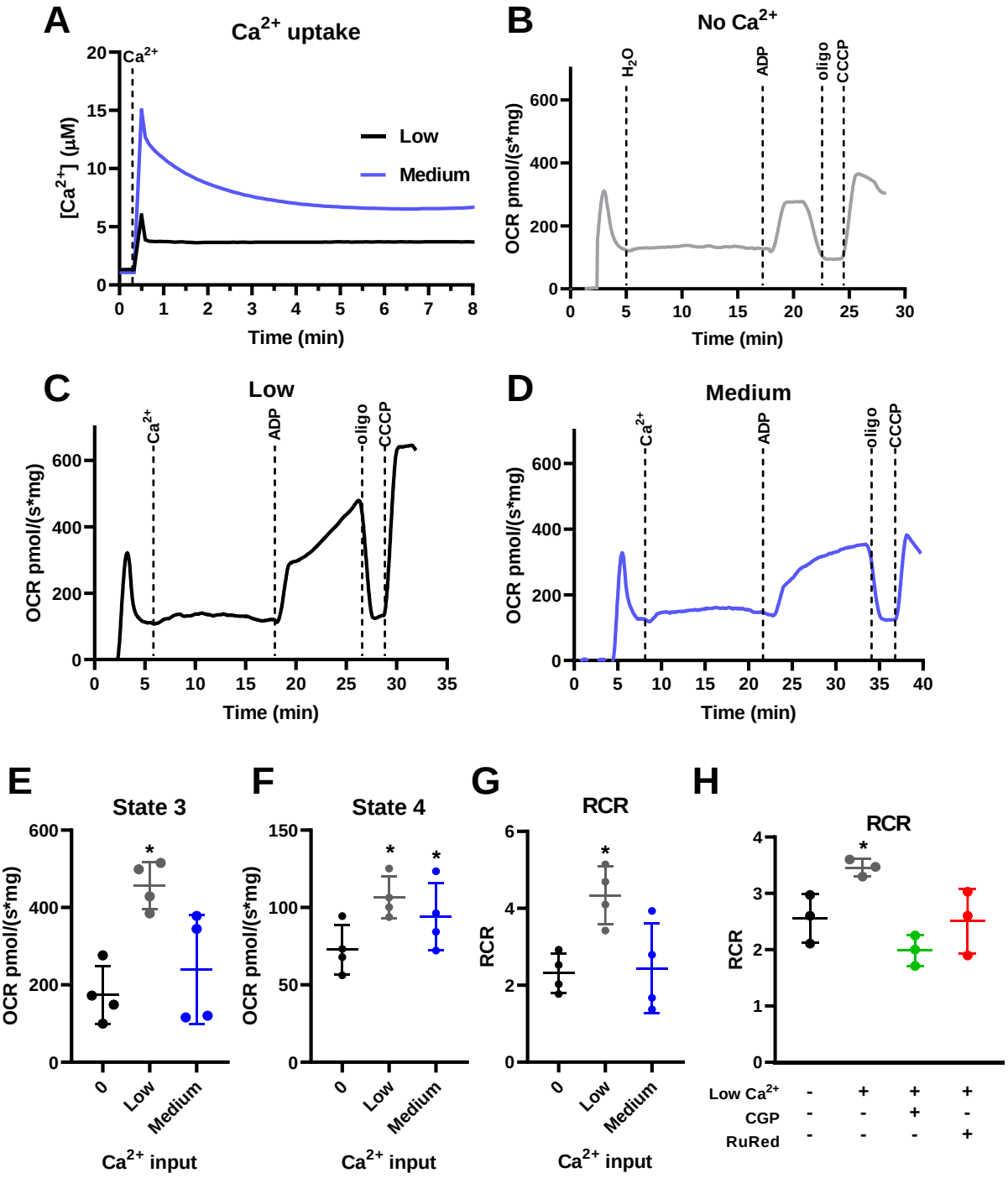


Vilas-Boas et al., 2022, Fig. 1

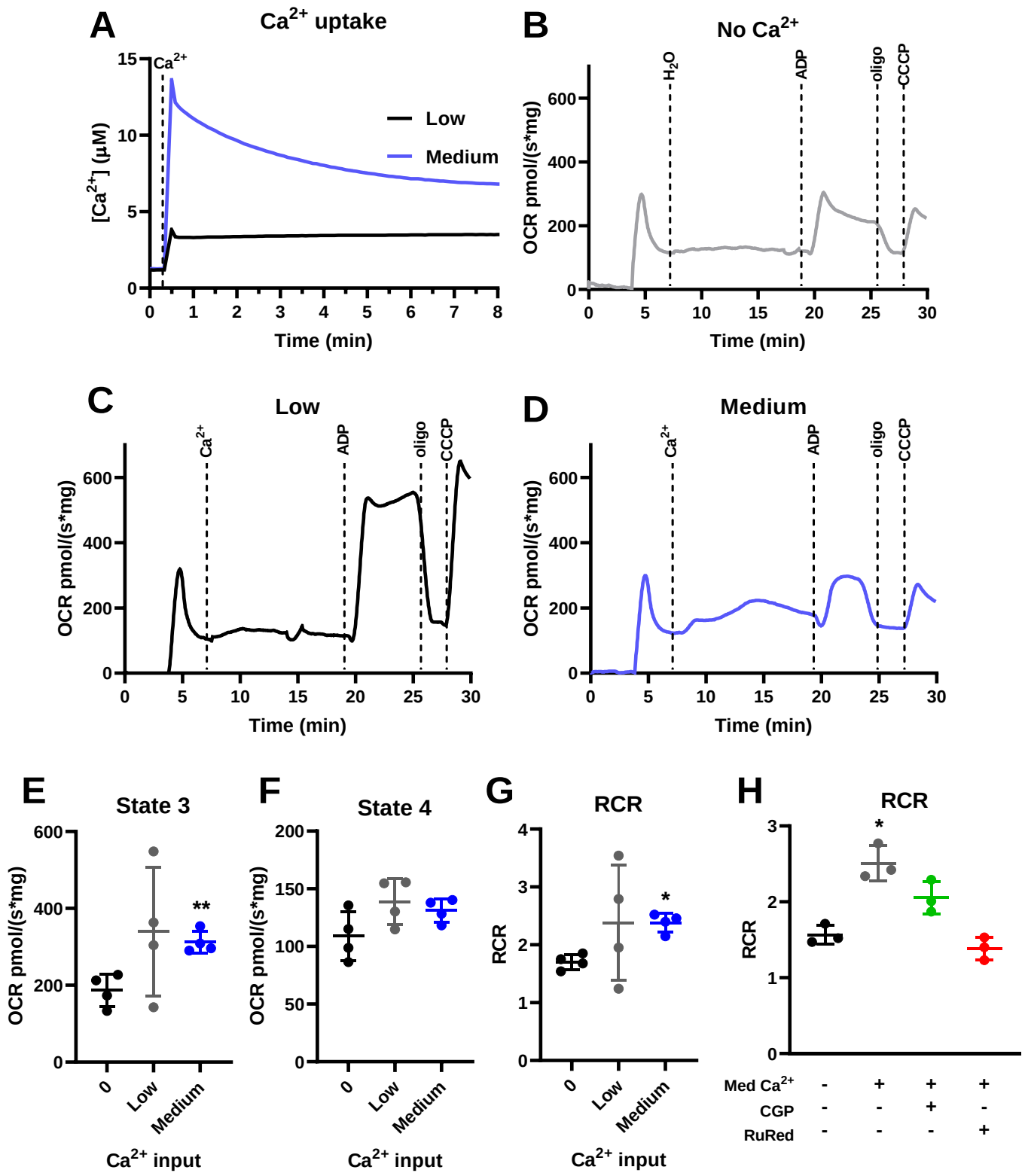


Vilas-Boas et al., 2022, Fig. 2

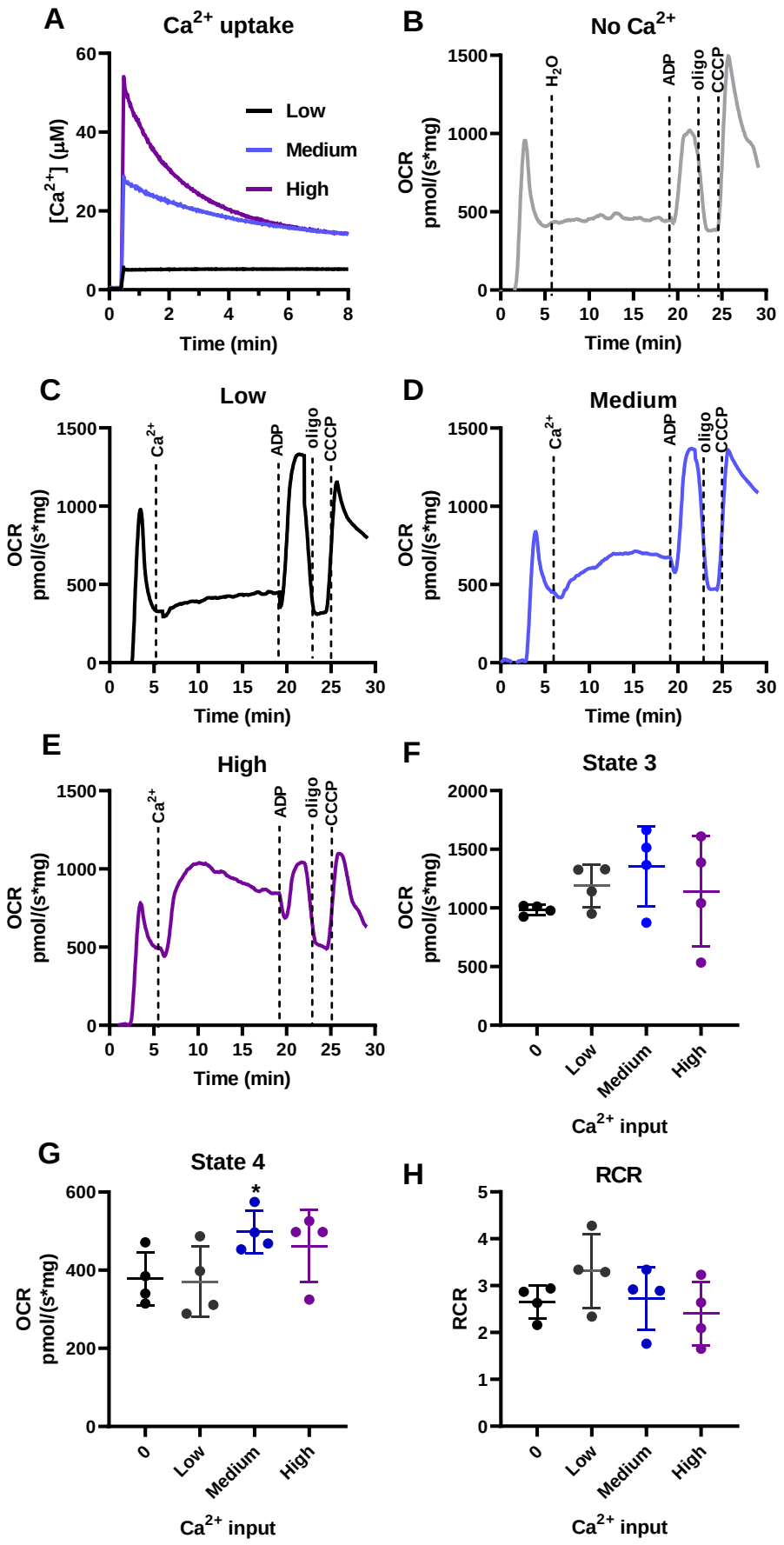


Vilas-Boas et al., 2022, Fig. 3

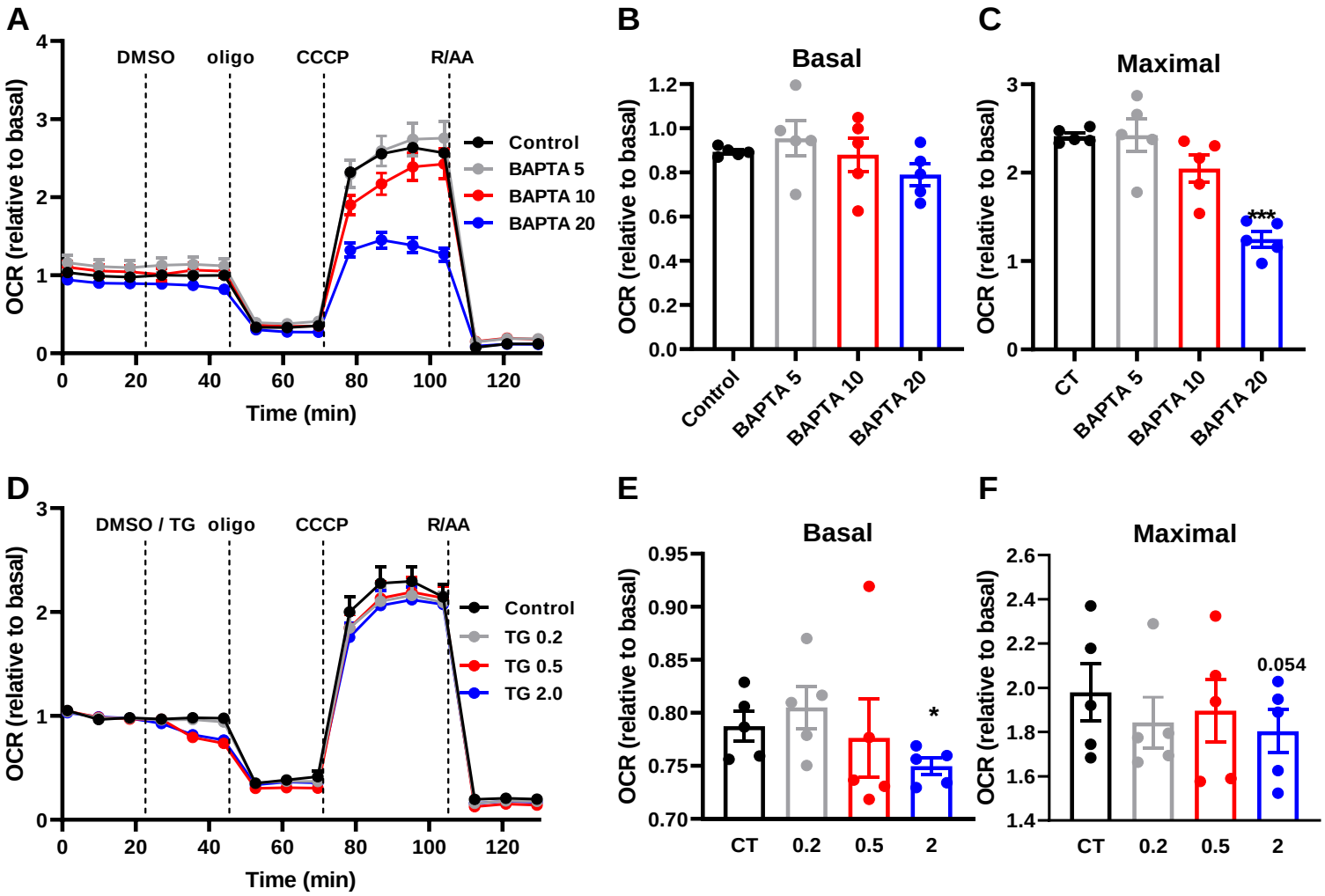


Vilas-Boas et al., 2022, Fig. 4

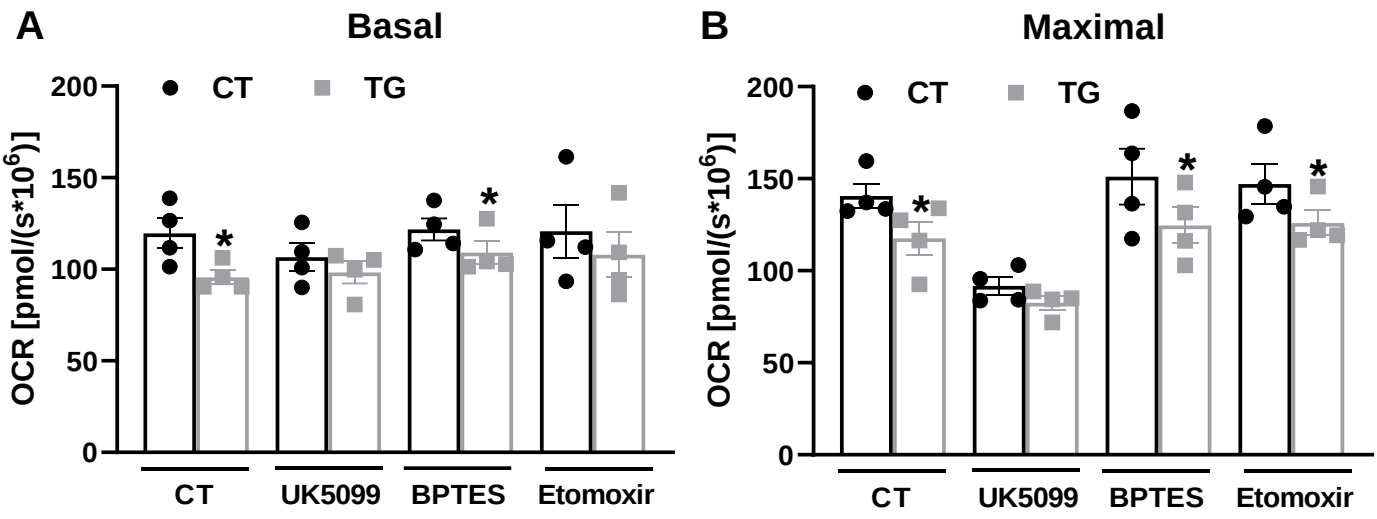


Vilas-Boas et al., 2022, Fig. 5

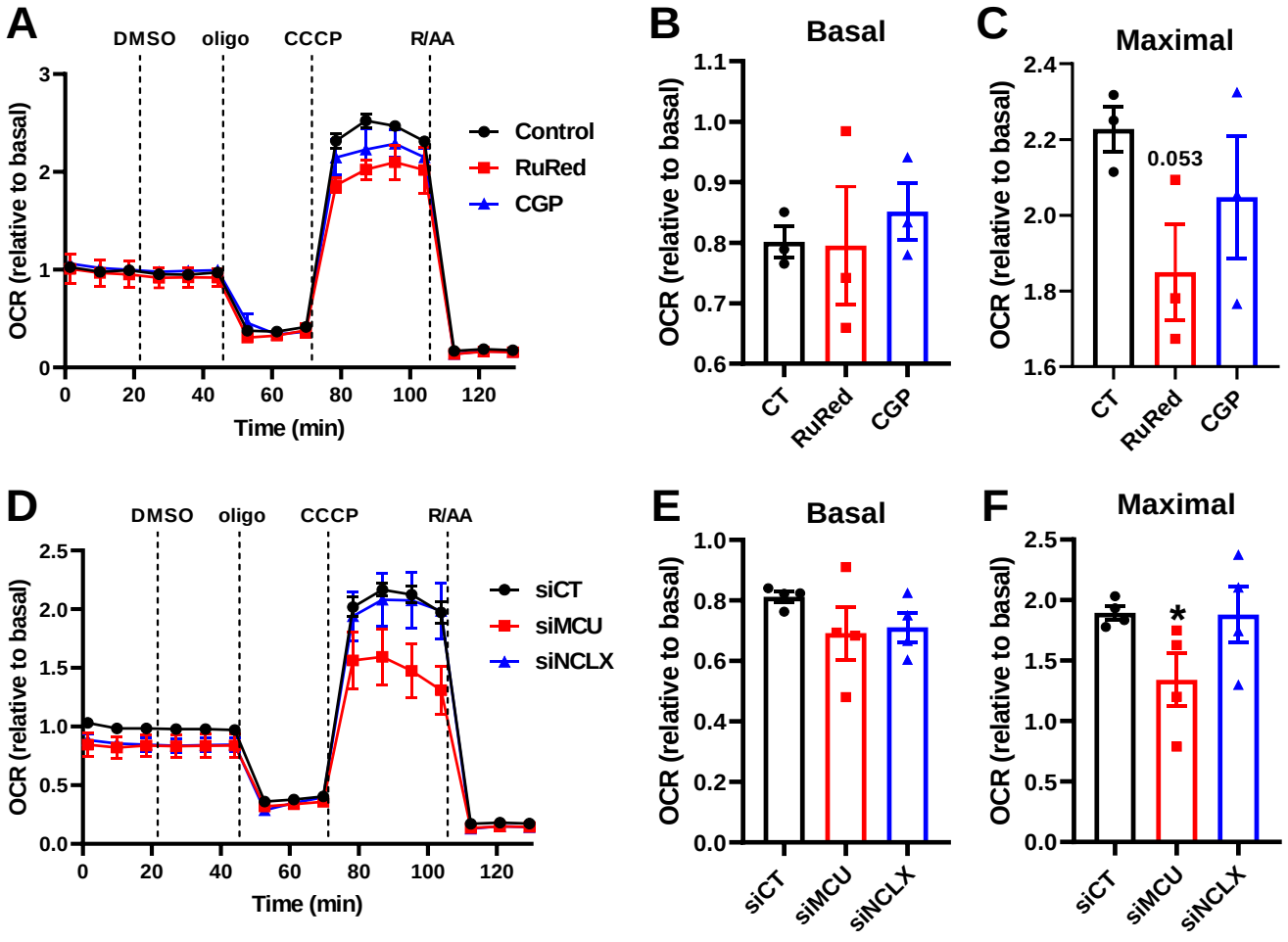


Vilas-Boas et al., 2022, Fig. 6

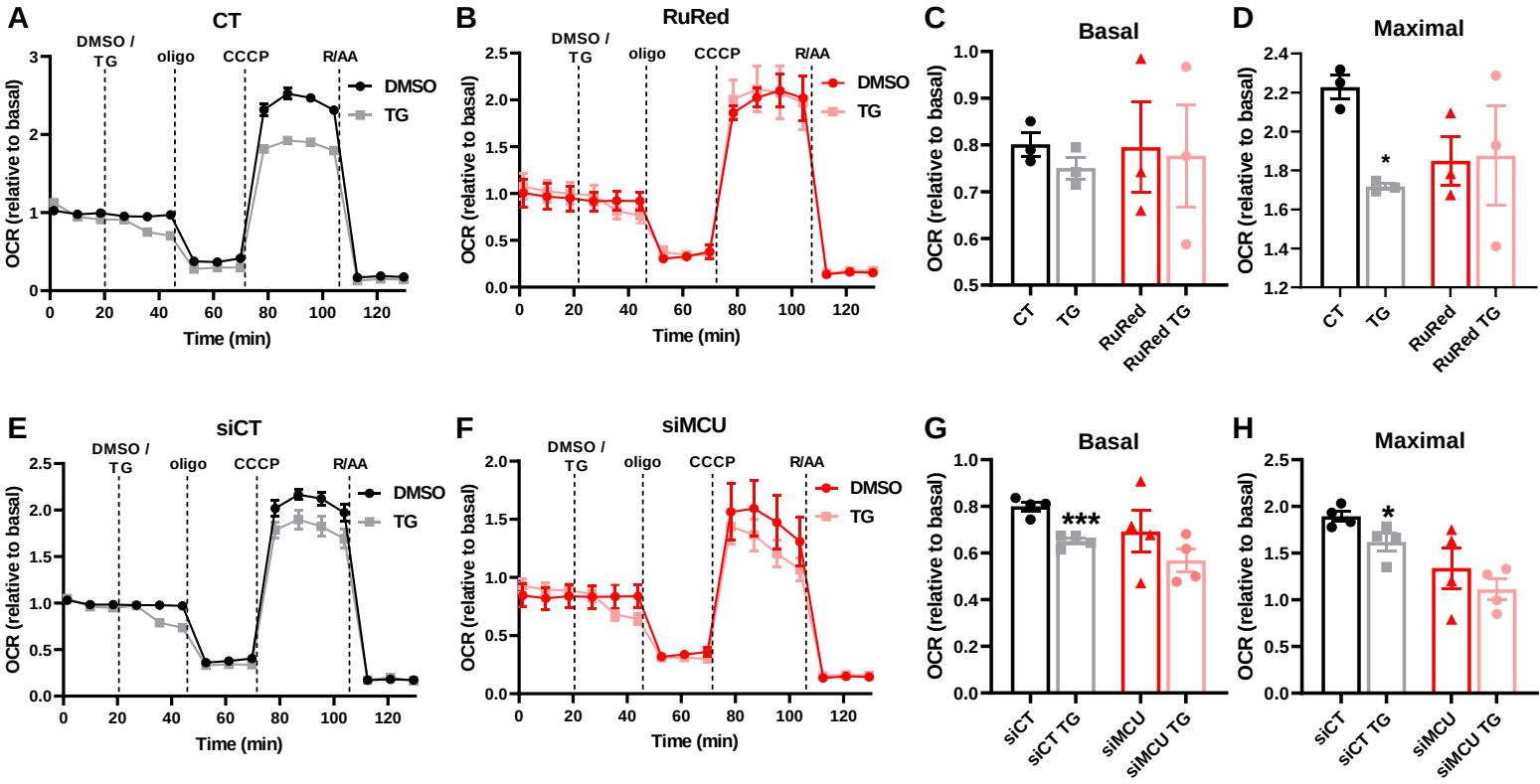


Vilas-Boas et al., 2022, Fig. 7

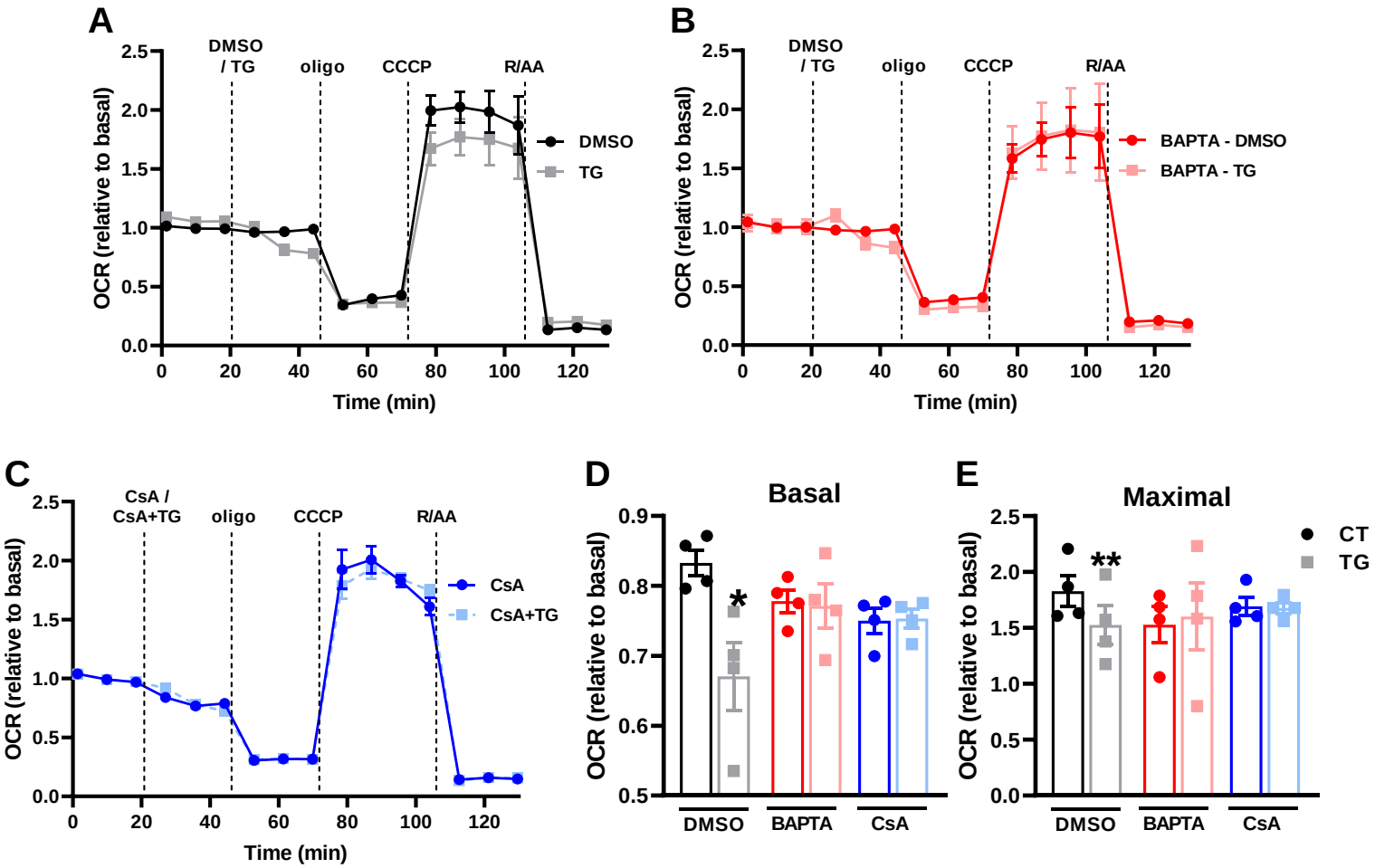


Vilas-Boas et al., 2022, Fig. 8

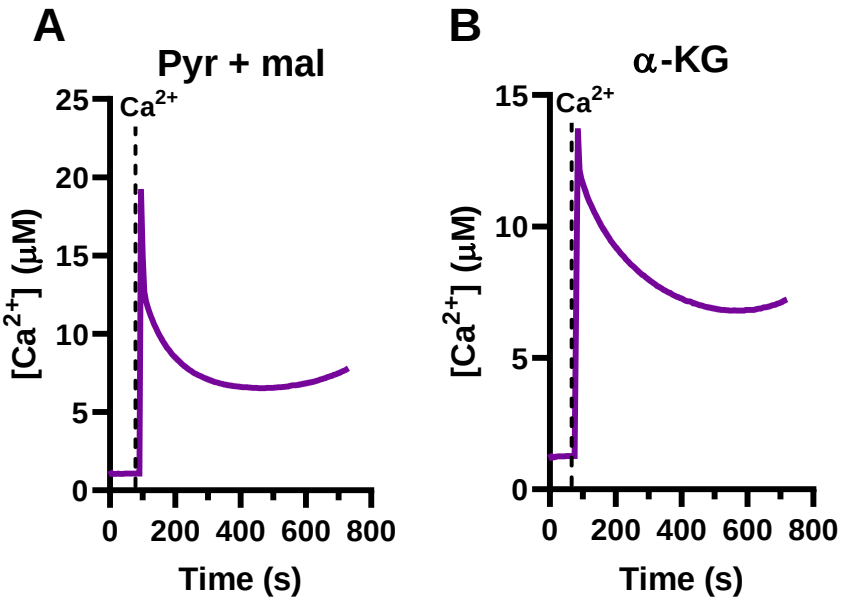


Vilas-Boas et al., 2022, Supplementary Fig. 1

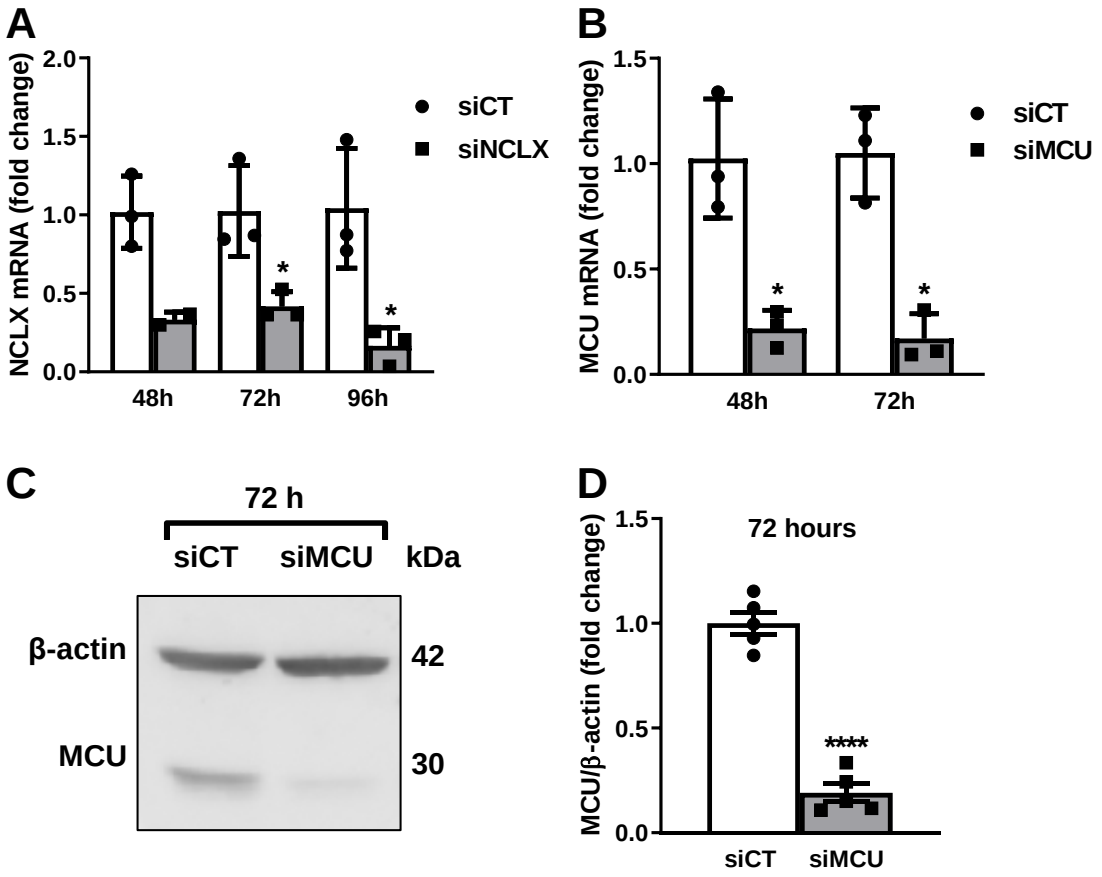


Vilas-Boas et al., 2022, Supplementary Fig. 2

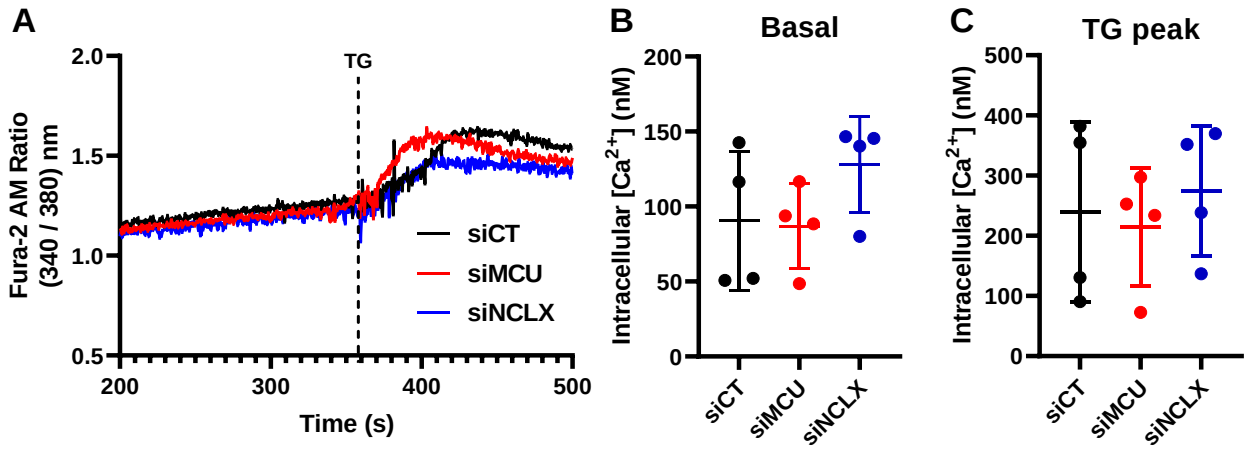


Vilas-Boas et al., 2022, Supplementary Fig. 3